Enhanced-Fidelity Ultrafast Geometric Quantum Computation Using Strong Classical Drives

Ye-Hong Chen,[1,2,3,4,*] Adam Miranowicz,[1,5] Xi Chen,[6,7] Yan Xia,[3,4] and Franco Nori[1,2,8]

[1] *Theoretical Quantum Physics Laboratory, Cluster for Pioneering Research, RIKEN, Wako-shi, Saitama 351-0198, Japan*

[2] *Quantum Information Physics Theory Research Team, Center for Quantum Computing, RIKEN, Wako-shi, Saitama 351-0198, Japan*

[3] *Fujian Key Laboratory of Quantum Information and Quantum Optics, Fuzhou University, Fuzhou 350116, China*

[4] *Department of Physics, Fuzhou University, Fuzhou 350116, China*

[5] *Institute of Spintronics and Quantum Information, Faculty of Physics, Adam Mickiewicz University, Poznań 61-614, Poland*

[6] *Department of Physical Chemistry, University of the Basque Country UPV/EHU, Apartado 644, Bilbao 48080, Spain*

[7] *EHU Quantum Center, University of the Basque Country UPV/EHU, Barrio Sarriena, s/n, Leioa 48940, Spain*

[8] *Department of Physics, University of Michigan, Ann Arbor, Michigan 48109-1040, USA*

(Received 20 March 2022; revised 23 September 2022; accepted 23 November 2022; published 20 December 2022)

We propose a general approach to implement ultrafast nonadiabatic geometric single- and two-qubit gates by employing counter-rotating effects. This protocol is compatible with most optimal control methods used in previous rotating-wave approximation (RWA) protocols; thus, it is as robust as (or even more robust than) the RWA protocols. Using counter-rotating effects allows us to apply strong drives. Therefore, we can improve the gate speed by 5–10 times compared to the RWA counterpart for implementing high-fidelity ($\geq$ 99.99%) gates. Such an ultrafast evolution (nanoseconds, even picoseconds) significantly reduces the influence of decoherence (e.g., the qubit dissipation and dephasing). Moreover, because the counter-rotating effects no longer induce a gate infidelity (in both the weak and strong driving regimes), we can achieve a higher fidelity compared to the RWA protocols. Therefore, in the presence of decoherence, one can implement ultrafast geometric quantum gates with $\geq$ 99% fidelities.

DOI: 10.1103/PhysRevApplied.18.064059

I. INTRODUCTION

Quantum computers promise to drastically outperform classical computers on certain problems, such as factoring, (approximate) optimization, boson sampling, or unstructured database searching [1–7]. To realize a quantum computer, one key ingredient is to realize high-fidelity quantum gates, especially, single- and two-qubit gates. This is because any unitary transformations, including multiqubit gates, can be decomposed into a series of single-qubit operations along with universal two-qubit gates (see, e.g., Refs. [4,5,8–18]). However, gate infidelities, due to decoherence, impede the physical implementation of large-scale quantum computers [3]. Many efforts have been made to solve the above problems. Among them, quantum geometric gates [19–39], based on Abelian [40] and non-Abelian [41,42] geometric phases, have become promising because geometric phases are determined by the global properties of the evolution paths and are intrinsically noise resilient against certain types of local noises. For instance, it has been demonstrated [25,27,43] that geometric phases are robust against fluctuations described as Ornstein-Uhlenbeck processes, i.e., stationary, Gaussian, and Markovian noises, which have a Lorentzian spectrum.

However, a geometric gate is relatively slow because it consumes extra resources to eliminate dynamical phases. Noise may accumulate in a slow evolution, thus reducing the gate fidelity. Though some efforts have been made [26,33,44–49], only little progress has been achieved in speeding up the gates. In particular, working under the rotating-wave approximation (RWA), it is challenging to accelerate the gates using finite-interaction strengths, which are much smaller than the qubit transition frequency [39].

The above problem motivates us to employ counter-rotating terms (which are usually neglected in many previous protocols) for nonadiabatic geometric quantum

*yehong.chen@riken.jp

computation (NGQC), so that one can apply strong interactions to achieve ultrafast and high-fidelity computation [50–52].

In this paper, we propose a general approach for ultrafast NGQC using driven two-level systems. Using strong drivings effectively shortens the gate time to nanoseconds (even picoseconds), and, thus, significantly reduces the influence of decoherence [53–59]. The effective Hamiltonian obtained by the Floquet theory [60,61] possesses a RWA-like form. Thus it is compatible with most optimal control methods [33,36–38,48,62–66], which have been applied under the RWA, such as the recently developed methods of super-robust geometric control [38] and doubly geometric quantum control [37].

The proposed protocol can avoid the negative effects caused by the counter-rotating (CR) interactions, including the Bloch-Siegert (BS) shift, which may shift the qubit transition frequency and induce additional systematic noise in the system. Thus, this protocol can suppress systematic noise better than the usual RWA counterpart. We also generalize the protocol to, e.g., two-qubit holonomic gates, using strong qubit-qubit couplings. Therefore, this protocol can be a possible replacement for conventional RWA methods, and to improve the speed and fidelity of the NGQC. Our approach is different from previous non-RWA protocols, e.g., Refs. [50–52,67–69], which work for specific targets.

II. EFFECTIVE HAMILTONIAN UNDER STRONG DRIVES

We consider a two-level atom (with ground state $|g\rangle$ and excited state $|e\rangle$) driven by a two-tone drive with the same frequency ω, different amplitudes $\Omega_n(t)$, and phases ϕ_n $(n = 0, 1)$. The Hamiltonian reads (hereafter, $\hbar = 1$)

$$H(t) = \frac{\omega_q}{2}\sigma_z + \sum_{n=0,1} \Omega_n(t)\cos(\omega t + \phi_n)\sigma_x, \tag{1}$$

where σ_η $(\eta = x, y, z, +, -)$ are Pauli matrices. For weak drivings (i.e., $\Omega_n \ll \omega, \omega_q$), we can perform

$$\begin{aligned} H_I &= \exp\left(\frac{i}{2}\omega t\sigma_z\right)\left[H(t) - \frac{\omega}{2}\sigma_z\right]\exp\left(-\frac{i}{2}\omega t\sigma_z\right) \\ &= \sum_n \left[\frac{e^{i\phi_n}\Omega_n(t)}{2}\left(1 + e^{2i\omega t}\right)\sigma_- + \text{h.c.}\right] + \frac{\Delta_q(t)}{2}\sigma_z, \end{aligned} \tag{2}$$

where $\Delta_q = \omega_q - \omega$ is the detuning. The fast-oscillating term with $\exp(\pm 2i\omega t)$ can be neglected under the RWA, and the effective Hamiltonian becomes

$$H_{\text{RWA}}(t) = \frac{\Delta_q(t)}{2}\sigma_z + \sum_n \frac{\Omega_n(t)}{2}\left(e^{i\phi_n}\sigma_- + \text{h.c.}\right). \tag{3}$$

This Hamiltonian has been widely applied to holonomic computation [39]. However, the condition $\Omega_n \ll \omega, \omega_q$ limits the gate speed. When we choose a relatively strong driving amplitude, e.g., $\Omega_n \sim 0.1\omega$, the neglected CR effect (which includes the BS shift) can induce an infidelity (see the black-dashed-dotted curve in Fig. 1). Here, the BS shift calculated by the second-order process is

$$H_{\text{BS}} = \sigma_z \sum_n \frac{\Omega_n^2(t)}{8\omega}. \tag{4}$$

Accordingly, the effective Hamiltonian becomes

$$H_{\text{RWA-BS}}(t) = H_{\text{RWA}}(t) + H_{\text{BS}}. \tag{5}$$

For simplicity, the RWA-based protocol considering the BS shift is denoted hereafter as the "RWA-BS" protocol. When this BS shift is considered, the phase mismatch can be fixed (see the green-dotted curve in Fig. 1). However, the actual dynamics (red-solid curve) is still not in good agreement with the effective dynamics (green-dotted curve).

To implement NGQC with the CR terms, we transform the Hamiltonian $H(t)$ with a time-dependent generator [60,61]

$$\begin{aligned} S(t) &= \exp\left[i\frac{Z}{2}\sin(\tau)\sigma_x\right], \\ \tau &= \omega t + \phi_0, \end{aligned} \tag{6}$$

resulting in

$$\begin{aligned} H'(t) &= S(t)H(t)S^\dagger(t) - iS(t)\dot{S}^\dagger(t) \\ &= \frac{\omega_q}{2}\cos\left[Z\sin(\tau)\right]\sigma_z \\ &\quad + \frac{\omega_q}{2}\sin\left[Z\sin(\tau)\right]\sigma_y \\ &\quad + \left[\Omega_0(t) - \frac{Z}{2}(\omega + \dot{\phi}_0)\right]\cos(\tau)\sigma_x \\ &\quad - \frac{\dot{Z}}{2}\sin(\tau)\sigma_x + \Omega_1(t)\cos(\omega t + \phi_1)\sigma_x, \end{aligned}$$

with a real time-dependent parameter Z to be determined below. The last-line expression in $H'(t)$ can be removed by choosing $\Omega_1 = \dot{Z}/2$ and $\phi_1 = \phi_0 - \pi/2$. Then, using the identity

$$\exp\left[iZ\sin(\tau)\right] = \sum_{m=-\infty}^{+\infty} J_m(Z)\exp(im\tau), \tag{7}$$

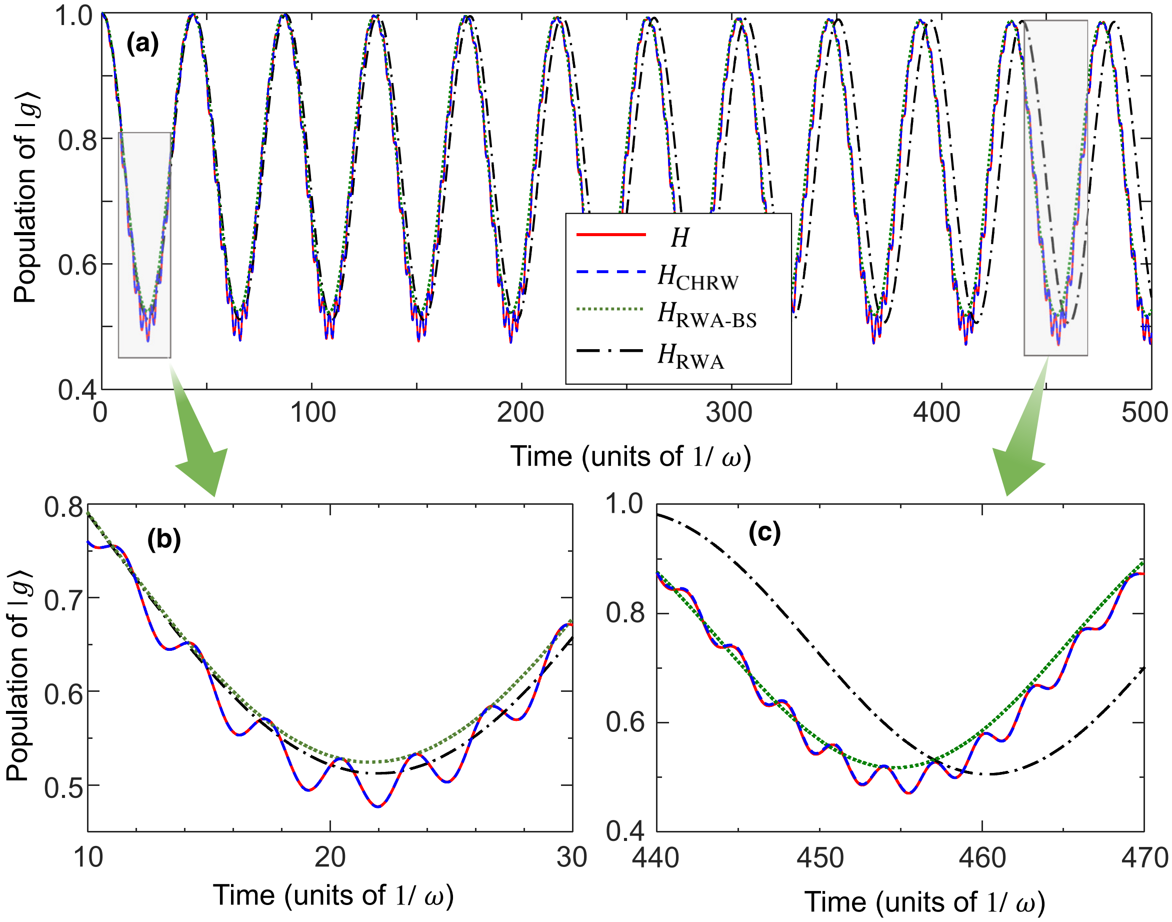

FIG. 1. Population of the ground state $|g\rangle$ in the laboratory frame governed by the Hamiltonians under different approximation protocols: $H(t)$ in Eq. (1), $H_{\rm CHRW}(t)$ in Eq. (12), $H_{\rm RWA}(t)$ in Eq. (3), and $H_{\rm RWA\text{-}BS}(t)$ in Eq. (4). We choose parameters $\tilde{\Delta}_q = \Delta_q = 0.1\omega$, $\Omega_0 = 0.1\omega$, and $\Omega_1 = 0$. Note that each curve is calculated using the corresponding Hamiltonian after its transformation back to the laboratory frame.

the Hamiltonian $H'(t)$ becomes

$$\begin{aligned} H'(t) &= H'_0(t) + H'_1(t) + H'_2(t), \\ H'_0(t) &= \frac{\omega_q}{2} J_0(Z)\sigma_z, \\ H'_1(t) &= \tilde{\Omega}_0(t)\cos(\tau)\sigma_x + \omega_q J_1(Z)\sin(\tau)\sigma_y, \\ H'_2(t) &= \omega_q \sum_{m=1}^{\infty} J_{2m+1}(Z)\sin[(2m+1)\tau]\sigma_y \\ &\quad + \omega_q \sum_{m=1}^{\infty} J_{2m}(Z)\cos(2m\tau)\sigma_z, \end{aligned} \tag{8}$$

where $J_m(Z)$ is the mth-order Bessel function of the first kind and

$$\tilde{\Omega}_0(t) = \left[\Omega_0(t) - \frac{Z}{2}(\omega + \dot{\phi}_0)\right], \tag{9}$$

is the effective driving amplitude. The Hamiltonian $H'_2(t)$ includes all higher-order harmonic terms, which can be neglected for $Z \in [0, 1]$ [57]. Note that this transformation is also valid for multilevel systems by defining a suitable generator $S(t)$ [53,56,59]. By assuming

$$\tilde{\Omega}_0(t) = \omega_q J_1(Z), \tag{10}$$

the effective Hamiltonian for the system now reads

$$\begin{aligned} H_{\rm eff}(t) &= H'_0(t) + H'_1(t) \\ &= \frac{\omega_q}{2} J_0(Z)\sigma_z + \tilde{\Omega}_0(t)\left(e^{i\tau}\sigma_- + {\rm h.c.}\right), \end{aligned} \tag{11}$$

which possesses a RWA-like form. Because this Hamiltonian contains some counter-rotating terms, which are neglected in the standard RWA protocols, we denote it as a counter-rotating hybridized rotating wave (CHRW) Hamiltonian [55,57]. By expanding $\exp[i\omega t\sigma_z/2]$, we obtain

$$\begin{aligned} H_{\mathrm{CHRW}}(t) =& e^{i\omega t\sigma_z/2} H_{\mathrm{eff}}(t) e^{-i\omega t\sigma_z/2} \\ =& \frac{\tilde{\Delta}_q(t)}{2}\sigma_z + \tilde{\Omega}_0(t)\left[e^{i\phi_0}\sigma_- + \mathrm{h.c.}\right], \end{aligned} \tag{12}$$

which takes the same form as Eq. (3) assuming $n = 0$. Here,

$$\tilde{\Delta}_q(t) = \omega_q J_0(Z) - \omega, \tag{13}$$

is the effective detuning, $\omega_q J_0(Z)$ is the renormalized transition frequency of the qubit, and $\tilde{\Omega}_0(t)$ is the effective driving amplitude. The renormalized quantities in the transformed Hamiltonian are directly induced by the CR effects. As shown in Fig. 1, the dynamics of the CHRW Hamiltonian $H_{\mathrm{CHRW}}(t)$ (after its transformation back to the laboratory frame) is mostly the same as that of the actual Hamiltonian $H(t)$.

According to Eqs. (8) and (10), the limitation on the effective driving strength $\tilde{\Omega}_0(t)$ is

$$\tilde{\Omega}_0(t) \ll \mathrm{Min}\left[\frac{4J_1(Z)m\omega}{J_{2m}(Z)}\right] \ll \frac{4\omega J_1(1)}{J_2(1)} \approx 15\omega, \tag{14}$$

In contrast to Eq. (14), the limitation on the RWA protocol is

$$\frac{\Omega_0(t)}{2} \ll 2\omega. \tag{15}$$

That is, the CHRW protocol can be approximately 7.5 times *faster* than the RWA protocol because the speed of the protocol is inversely proportional to the effective driving strength (i.e., the left-hand sides of the inequalities).

To check the range of validity of the above approximations, we define an initial-state-independent fidelity [70,71]

$$\bar{F} = \left[\mathrm{Tr}(MM^\dagger) + |\mathrm{Tr}(M)|^2\right]/(D^2 + D),$$

where,

$$M = \mathcal{P}_c U^\dagger_{\mathrm{eff}}(t) U_{\mathrm{act}}(t)\mathcal{P}_c, \tag{16}$$

and $\mathcal{P}_c$ ($D = 2$) is the projector (dimension) of the qubit subspace. The evolution operators $U_{\mathrm{eff}}(t)$ and $U_{\mathrm{act}}(t)$ describe the effective and actual dynamical evolutions governed by the approximate Hamiltonian [$H_{\mathrm{RWA}}(t)$ or $H_{\mathrm{CHRW}}(t)$] and the total Hamiltonian $H(t)$, respectively.

Note that the CR effect always influences the system dynamics. To show clearly such influences in a long-time evolution, we define an average fidelity, $\mathcal{F} = 1/T\int_0^T dt\bar{F}$, which averages the fidelities $\bar{F}$ over time, where T is the total evolution time. This average fidelity evaluates well the error caused by the CR effect. Moreover, because $U_{\mathrm{act}}(t)$ describes a set of universal quantum gates, $\bar{F}$ is also the average fidelity of this set of gates.

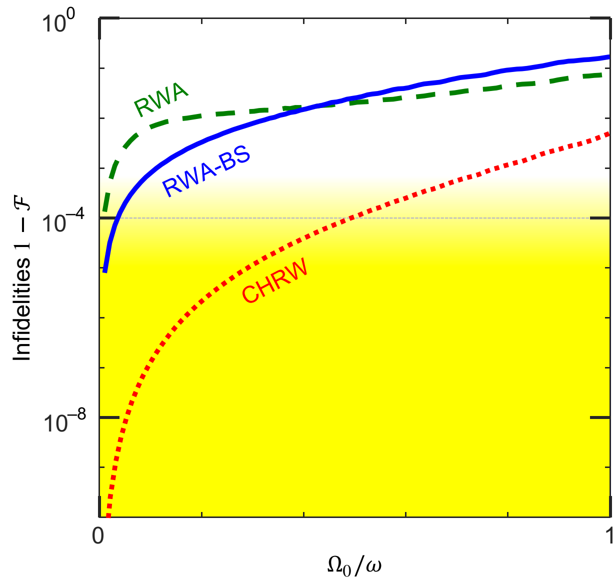

FIG. 2. Infidelities $(1 - \mathcal{F})$ averaged over time of the CHRW, RWA-BS, and RWA protocols for $T = 100/\Omega_0$ with Hamiltonians $H_{\mathrm{CHRW}}(t)$ in Eq. (12), $H_{\mathrm{RWA}}(t)$ in Eq. (3), and $H_{\text{RWA-BS}}(t)$ in Eq. (4), respectively. We choose $\Omega_0(t) = \mathrm{const}$, $\Delta_q(t) = \tilde{\Delta}_q(t) = 0.1\omega$, and $\phi_0 = 0$. For the RWA and RWA-BS protocols, we choose $\Omega_1(t) = 0$. Hereafter, all the yellow-shaded areas in the figures correspond to high fidelities ($\gtrsim$ 99.99%); and numerical results are calculated using the Hamiltonian $H(t)$ in Eq. (1).

For $\mathcal{F} = 1$, the effective dynamics is exactly the same as the actual one. Using this definition, in Fig. 2, we show that for $\Omega_0(t) \sim \omega/2$ (a strong driving), the CHRW protocol (see the red-dotted curve) is valid to describe the system dynamics, while the RWA (see the green-dashed curve) is invalid even when the BS shift is considered (blue-solid curve). Such a strong driving can significantly accelerate the evolution, allowing ultrafast quantum computation. Note that the BS shift obtained by the second-order process is valid only for $\Omega_0(t) \ll \omega$. For $\Omega_0(t) > \omega/2$, it may induce a greater infidelity [see the blue-solid curve in Fig. 1(a)] even compared to the RWA protocol.

III. IMPLEMENTING FAST NONADIABATIC GEOMETRIC GATES

Obviously, $H_{\mathrm{CHRW}}(t)$ in Eq. (12) has exactly the same form as $H_{\mathrm{RWA}}(t)$ in Eq. (3). Therefore, the proposed protocol is compatible with the majority of the pulse-design methods [22,23,31,34,36–38], which have been applied for geometric quantum computation under the RWA. For a cyclic evolution, we can choose the gate time $T = k\pi/\omega$ ($k = 1, 2, 3, \ldots$) and $S(0) = S(T) = 1$, so that the unitary transformations do not affect the geometric property of the evolution [40–42].

According to the Lewis-Riesenfeld theory [72], the evolution of the system governed by $H_{\mathrm{CHRW}}(t)$ can be described as [73–77] (see more details in Appendix A),

$$|\phi_+(t)\rangle = e^{i\mathcal{R}_+(t)}\left[ie^{-i\alpha}\sin(\beta/2),\ \cos(\beta/2)\right]^{\mathrm{T}}, \tag{17}$$

or its orthogonal counterpart

$$|\phi_-(t)\rangle = e^{i\mathcal{R}_-(t)}\left[\cos(\beta/2),\ ie^{i\alpha}\sin(\beta/2)\right]^{\mathrm{T}}. \tag{18}$$

Here, $\mathcal{R}_\pm(t)$ are the Lewis-Riesenfeld phases, including dynamical and geometric phases, α and β are auxiliary parameters to be determined below, and the superscript “T” is the transposition operator.

To eliminate the dynamical phase, we can choose the parameters $\tilde{\Delta}_q(t) = -\dot{\alpha}\sin^2\beta$, and

$$\begin{aligned}\tilde{\Omega}_0(t)\cos\phi_0 &= \frac{1}{4}\left[\dot{\alpha}\sin(2\beta)\sin\alpha - 2\dot{\beta}\cos\alpha\right],\\ \tilde{\Omega}_0(t)\sin\phi_0 &= \frac{1}{4}\left[\dot{\alpha}\sin(2\beta)\cos\alpha + 2\dot{\beta}\sin\alpha\right],\end{aligned} \tag{19}$$

resulting in

$$\langle\phi_\pm(t)|H_{\mathrm{CHRW}}(t)|\phi_\pm(t)\rangle = 0. \tag{20}$$

Moreover, the equations of motion for the geometric phases read

$$\dot{\Theta}_\pm(t) = \pm\dot{\alpha}\sin^2(\beta/2). \tag{21}$$

Hence, after a cyclic evolution, which is obtained by choosing $\alpha(T) = \alpha(0) \pm 2n_\alpha\pi$ and $\beta(T) = \beta(0) \pm 4n_\beta\pi$ [$n_{\alpha(\beta)} = 0, 1, 2, \ldots$], the evolution operator at the gate time T becomes

$$U_{\mathrm{eff}}(T) = \sum_{k=\pm}\exp\left[i\Theta_k(T)\right]|\phi_k(0)\rangle\langle\phi_k(0)|, \tag{22}$$

which is a universal single-qubit gate.

In this paper, we focus on how the CR effects can shorten the gate time. Therefore, for simplicity, we choose time-dependent parameters

$$\begin{aligned}\alpha &= \alpha(0) + \pi\left[1 - \cos(\pi t/T)\right],\\ \beta &= \beta(0) + \Lambda\sin^2(\pi t/T),\end{aligned} \tag{23}$$

so that $S(0) = S(T) = 1$, where the parameter Λ is numerically obtained according to the geometric phases $\Theta_\pm(T)$. The parameters chosen for implementing some single-qubit gates are listed in Table I. Thus, substituting Eq. (23) into Eq. (19), we can numerically obtain the expressions

TABLE I. Parameters used for the examples implementing single-qubit gates.

Gate	$\alpha(0)$	$\beta(0)$	$\Theta_+(T)$	Λ
NOT	$\pi/2$	$\pi/2$	$\pi/2$	0.8089
Hadamard	$\pi/2$	$\pi/4$	$\pi/2$	0.3867
Phase π	0	0	$\pi/2$	1.4669

for Z and ϕ_0, and, afterwards, the driving amplitudes $\Omega_0(t)$ and $\Omega_1(t)$.

According to the fiber bundle theory, different frames can have all well-defined geometric quantities [40–42]. Indeed, the geometric phases defined in different frames satisfy the same property, which is essential to the definition of geometric phases, i.e., they are invariant under distinct connections and gauge potentials.

For instance, to implement the Hadamard gate using the parameters listed in Table I, the numerical solutions for Z and ϕ_0 are shown in Fig. 3(a). Accordingly, we show the driving amplitudes and detuning in Fig. 3(b). For $T = 5\pi/\omega$, the peak value of the driving amplitude $\Omega_0(t)$ is approximately 0.15ω. With such a strong driving, the RWA becomes invalid to obtain a high-fidelity ($\bar{F}_H \gtrsim 99.99\%$) Hadamard gate [see the green-dashed and blue-solid curves in Fig. 4]. Note that a functional quantum gate should be very precise, typically with a relative error $\lesssim 10^{-4}$ [see the yellow-shaded area in Fig. 4] [78].

In contrast to this, the CHRW protocol can implement high-fidelity quantum gates using strong drivings. As a result, the gate time of the Hadamard gate can be shortened to $T \sim 5\pi/\omega$. Considering an implementation of the CHRW protocol using natural or artificial atoms, the driving frequency is $\omega \sim 2\pi \times 5$ GHz and the gate time is only $T \sim 0.5$ ns.

Note from Eqs. (19) and (23) that the effective driving amplitude $\tilde{\Omega}_0(t)$ is inversely proportional to the gate

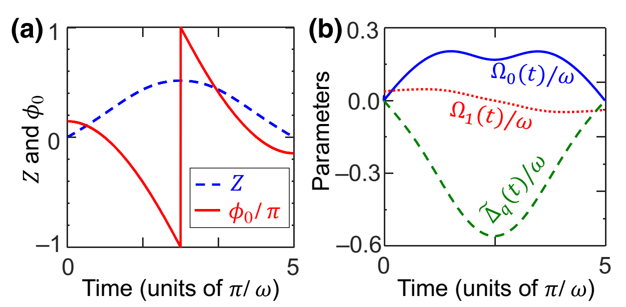

FIG. 3. Implementations of the Hadamard gate using the parameters in Table I. The parameters shown in (a),(b) are for the CHRW protocol when $T = 5\pi/\omega$. The driving amplitude $\Omega_0(t)$ is comparable to the qubit transition frequency ω_q with these parameters.

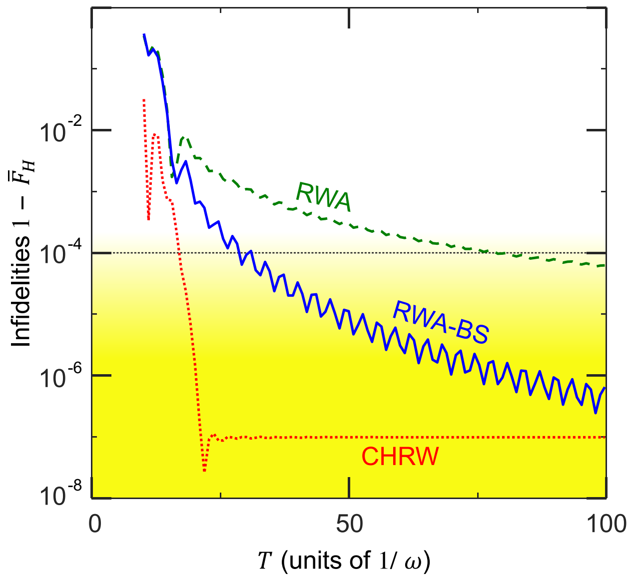

FIG. 4. Comparisons of infidelities $(1-\bar{F}_H)$ for the three protocols. For a fixed gate time T, the RWA protocol has the highest infidelities, while the CHRW protocol has by far the lowest infidelities. For the RWA and RWA-BS protocols, we choose $\Omega_1(t)=0$.

time T. Therefore, instead of discussing the driving amplitude, analyzing the gate time can highlight the advantages (e.g., speed) of the CHRW protocol. For implementing various quantum gates, the comparisons of the gate speeds for the CHRW, RWA-BS, and RWA protocols are shown in Table II. Generally, the shortest gate times to achieve high-fidelity gates for the CHRW protocol are 5–10 times shorter than those for the RWA protocol. The RWA-BS protocol also can improve the gate speed by 3–4 times, compared to the RWA protocol. These indicate that using the CR effects can effectively improve the gate speed for holonomic computation. For simplicity, the following discussions focus on the Hadamard gate.

IV. ROBUSTNESS AGAINST PARAMETER IMPERFECTIONS

Imperfections in the drives are a major source of noise for the discussed system. The parameter $X\in\left[\Omega_{0,(1)}(t),\Delta_q(t),\phi_{0,(1)},T\right]$ with these imperfections should be corrected as $X'=X\,(1\pm\delta X)$, where δX denotes the noise rates. For systematic noise, δX is a constant. For simplicity, we consider that the noise rates for different parameters are the same, i.e., $\delta\Delta_q(t)=\delta\Omega_0(t)$. In the presence of systematic noise, the gate infidelities for the three protocols are shown in Fig. 5(a), when choosing the same gate time $T=16\pi/\omega$. As shown, for small noise rates, the CHRW protocol can suppress systematic noise much better than the RWA protocol; and better than the RWA-BS protocol. Therefore, for small noise rates [e.g., $\delta\Omega_0(t)=\delta\delta_q(t)\lesssim\pm0.01$], it is still possible to implement quantum gates with fidelities $\gtrsim 99.99\%$.

TABLE II. The shortest gate time T (in units of π/ω) required to implement some high-fidelity ($\bar{F}\geq 99.99\%$) gates for different protocols.

Protocol	NOT	Hadamard	Phase π	CNOT-like
CHRW	~ 5	~ 6	~ 6	~ 5
RWA-BS	~ 8	~ 10	~ 10	~ 8
RWA	~ 34	~ 27	~ 48	~ 25

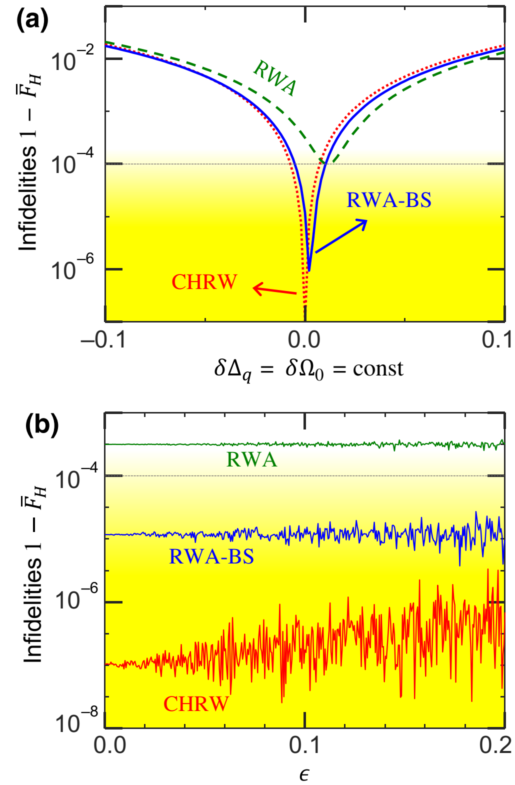

FIG. 5. Gate infidelities $(1-\bar{F}_H)$ of the CHRW, RWA-BS, and RWA protocols for the Hadamard gate. (a) In the presence of dynamical noise [i.e., $\delta\Delta_q(t)=\delta\Omega_0(t)$ are constants]. (b) In the presence of stochastic noise [i.e., $|\delta\Delta_q(t)|,|\delta\Omega_0(t)|\leq\epsilon$ are random numbers]. We choose the same gate time $T=16\pi/\omega$ for the three protocols, so that the driving amplitudes for different protocols are similar to each others. Other parameters are listed in Table I.

For stochastic noise, δX becomes a random number. We can assume $\delta X\in[-\epsilon,\epsilon]$ and numerically study its influence, where ϵ denotes the peak noise rate. Same as above, we now consider noise in $\Delta_q(t)$ and $\Omega_0(t)$, and show the gate infidelites $(1-\bar{F}_H)$ in Fig. 5(b). We find that stochastic noise affects the protocols very weakly. Such noise decreases the gate fidelities by approximately 10^{-4}, approximately 10^{-5}, and approximately 10^{-6} for the RWA (green curve), RWA-BS (blue curve), and CHRW (red curve) protocols, respectively. This shows that all the three protocols are robust against stochastic noise; and the CHRW protocol can be more robust than the other two.

V. DECOHERENCE

Note that an ultrafast evolution can significantly reduce the decoherence of a qubit. In the presence of decoherence [79,80], the system dynamics is described by the master equation

$$\dot{\rho} = -i[H(t), \rho] + \gamma\mathcal{D}[\sigma_-]\rho + \gamma_\phi\mathcal{D}[\sigma_z]\rho, \tag{24}$$

where

$$\mathcal{D}[o]\rho = o\rho o^\dagger - \frac{1}{2}\left(o^\dagger o\rho + \rho o^\dagger o\right) \tag{25}$$

is the standard Lindblad superoperator and γ (γ_ϕ) is the spontaneous emission (dephasing) rate. The fidelity of an output state $|\phi_{\rm out}\rangle$ is defined as $F_{\rm out} = \langle\psi_{\rm out}|\rho(T)|\psi_{\rm out}\rangle$.

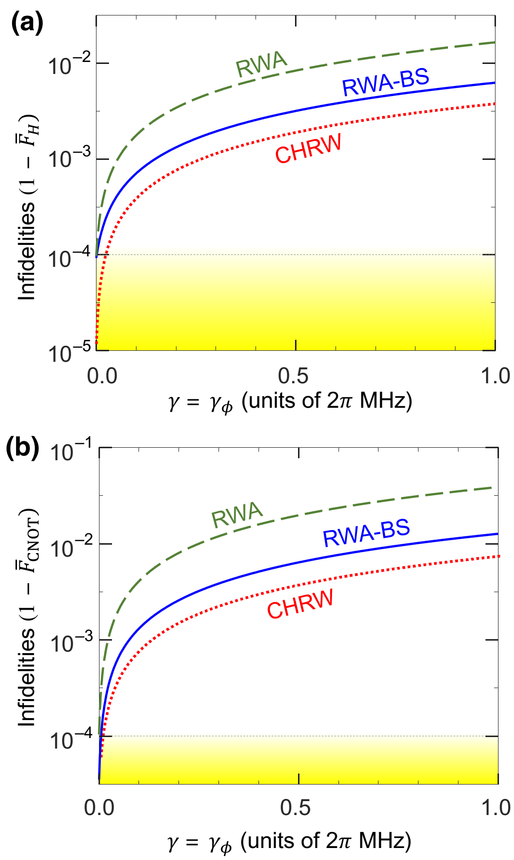

FIG. 6. Gate infidelities: (a) $1 - \bar{F}_H$ (Hadamard gate) and (b) $1 - \bar{F}_{\rm CNOT}$ (CNOT-like gate), averaged over 10 000 input states) of the CHRW, RWA-BS, and RWA protocols in the presence of decoherence. We choose the frequency $\omega = 2\pi \times 5$ GHz. Other parameters are listed in Tables I and II.

Thus, we redefine the gate fidelity $\bar{F}$ as the average value of $F_{\rm out}$ over many possible input states.

We can choose the driving frequency $\omega = 5$ GHz. In the presence of decoherence, comparisons of gate fidelities (averaged over 10 000 input states) among the three protocols are shown in Fig. 6(a). These input states are uniformly distributed over the Bloch sphere, which are defined as

$$|\psi\rangle_{\rm in} = \cos\theta_{\rm in}|g\rangle + \sin\theta_{\rm in}e^{i\varphi_{\rm in}}|e\rangle, \tag{26}$$

where $\theta_{\rm in} \in [0, 2\pi]$ and $\varphi_{\rm in} \in [0, 2\pi]$ are two parameters determining the input state. For simplicity, we choose $\theta_{\rm in}$ and $\varphi_{\rm in}$ as arithmetic progressions in the range $[0, 2\pi]$ and obtain the 10 000 input states. The comparison indicates that the CHRW approach can achieve much higher gate fidelities than the RWA-BS and the RWA protocols. Also, the RWA-BS protocol has higher fidelities than the RWA one. Moreover, for $\gamma = \gamma_\phi = 2\pi \times 0.025$ MHz (which has been realized using superconducting qubits [5,15,17,18,81,82]), the CHRW protocol can reach the threshold of 10^{-4} required for quantum error correction [83,84]. This is difficult for the RWA protocol to match because reaching a higher fidelity requires a longer gate time (see Fig. 4), which, however, increases the influence of decoherence. This is one reason why it is still difficult to experimentally realize a single-qubit geometric gate with fidelity $> 99.9\%$ based on the RWA protocols [35,85,86] (the coherence times of some superconducting qubits are now reaching 1 ms, as shown in Table III).

VI. TWO-QUBIT GATES

Two-qubit gates can be implemented with the evolution operator

$$\tilde{U}_{\rm eff}(t) = \frac{1}{2}\left(\mathbb{1}^a + \sigma_z^a\right) \otimes \mathbb{1} + \frac{1}{2}\left(\mathbb{1}^a - \sigma_z^a\right) \otimes U_{\rm eff}(t), \tag{27}$$

where $\mathbb{1}$ is the unit operator and the superscript a denotes the additional qubit. The parameters used for the single-qubit gates can be directly applied to the two-qubit gates. Hence, when $U_{\rm eff}(T) = i\sigma_x$, $\tilde{U}_{\rm eff}(T)$ corresponds to a CNOT-like gate. Based on the evolution operator $\tilde{U}_{\rm eff}(t)$, we can reversely deduce the corresponding effective Hamiltonian as

$$\tilde{H}_{\rm eff}(t) = i\dot{\tilde{U}}_{\rm eff}(t)\tilde{U}_{\rm eff}^\dagger(t) = \frac{1}{2}\left(\mathbb{1}^a - \sigma_z^a\right) \otimes H_{\rm eff}(t). \tag{28}$$

This effective Hamiltonian is an approximation of the reference Hamiltonian

$$\tilde{H}(t) = \frac{1}{2}\left(\mathbb{1}^a - \sigma_z^a\right) \otimes H(t), \tag{29}$$

which includes a dipole-dipole interaction $\sigma_z^a \otimes \sigma_z$ [87–89] and a tunable longitudinal coupling $\sigma_z^a \otimes \sigma_x$ [90–95].

TABLE III. Fidelities of geometric quantum gates using superconducting qubits. Coherence properties: energy relaxation time ($T_1 = 1/\gamma$) and dephasing time $T_2^* = 1/\gamma_\phi$. In our protocol, we calculate the gate fidelity by averaging over 10 000 input states, which are uniformly distributed over the Bloch sphere.

Year & Ref.	Gate type	$\omega_q/2\pi$ (GHz)	$\gamma/2\pi$ (kHz)	$\gamma_\phi/2\pi$ (kHz)	T_1 (μs)	T_2^* (μs)	Gate time (ns)	Fidelity (%)
2020 [35]	Single-qubit rotation gates	~ 4.61	~ 10	~ 16	~ 16	~ 10	80	~ 99.77
	Two-qubit rotation gates	112.8	~ 97.70					
2021 [85]	Single-qubit rotation gates	~ 5.62	~ 15	~ 29	~ 10.5	~ 5.5	100	~ 99.50
2021 [86]	Controlled-NOT gate	~ 5.58	~ 12	~ 13	~ 2.1	~ 73	205	~ 90.50
Our protocol	Single- and two-qubit gates	~ 5	~ 25	~ 25	~ 6.4	~ 6.4	0.5	$\gtrsim 99.99$

For the CNOT-like gate, the gate time to achieve a fidelity $\geq 99.99\%$ is similar to that of the NOT gate, i.e., $T \sim 5\pi/\omega$ for the CHRW protocol (see Table II). In the presence of decoherence, we assume that the two qubits have the same dissipation rates and show the gate fidelities in Fig. 6(b). As shown, the CHRW and the RWA-BS protocols have higher fidelities than those for the RWA protocol, indicating that employing CR effects can enhance the gate fidelities.

VII. DISCUSSIONS

The model discussed here is generic, so that the proposed proposal can be realized in a wide range of physical systems. One of the most promising devices to realize the CHRW protocol can be superconducting circuits [5,15,81,96–101], which have achieved strong interactions [15,100–102]. The needed time-dependent detuning or, equivalently, the time-dependent qubit transition frequency ω_q can be controlled in general, e.g., by Stark shifts. The CHRW protocol has a higher speed and a higher fidelity than those of the RWA-BS protocol, because the effective Hamiltonian includes high-order terms in the BS shift obtained by the Floquet theory [57,60,61]. As a result, even in the weak-driving regime, i.e., $\Omega_n(t) \ll \omega$, the CHRW protocol can achieve a higher fidelity than that for the RWA and RWA-BS protocols, as shown in Fig. 4. Note that to avoid the possible excitations to higher-energy levels, a system with strong anharmonicity should be used. Figure 7 shows the gate infidelities versus the frequency of the second-excited level of the atom. We can see that to achieve ultrafast quantum geometric gates using our CHRW protocol, a strong anharmonicity

$$\omega_2 - \omega_q \gtrsim 10\omega, \tag{30}$$

is needed, where ω_2 is the frequency of the second-excited level of the atom. In general, such a strong anharmonicity is possible using fluxonium and charge qubits [15,99–106].

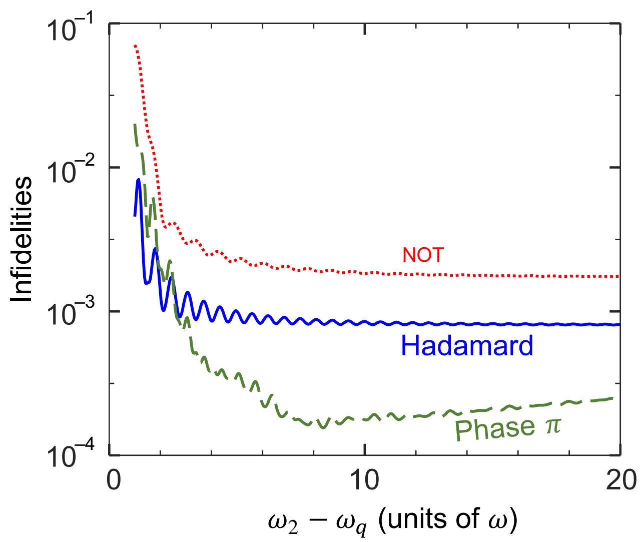

FIG. 7. Gate infidelities ($1 - \bar{F}$) of the CHRW protocol when the second-excited level (of frequency ω_2) of the atom is considered. Parameters for the plot are listed in Tables I and II.

VIII. POSSIBLE IMPLEMENTATION WITH SUPERCONDUCTING CIRCUITS

We now present a possible implementation with superconducting circuits for single-qubit gates. We consider a qubit circuit (see Fig. 8) formed by a capacitor C, an inductor L, and a Josephson junction with Josephson energy E_J. The qubit is controlled by an external current $I_{\text{out}}(t)$, which couples to the dimensionless flux variable Φ through a mutual inductance M. The system Hamiltonian is

$$\begin{aligned} H_{\text{SC}} =& H_0 + H_D, \\ H_0 =& 4E_C Q^2 + \frac{E_L}{2}\Phi^2 - E_J \cos\left(\Phi + \frac{\Phi_e}{\Phi_0}\right), \\ H_D =& \frac{M I_{\text{out}}(t)\Phi_0}{L}\Phi, \end{aligned} \tag{31}$$

where Q is the dimensionless charge operator, Φ is the dimensionless flux operator, $\Phi_0 = \hbar/(2e)$ is the reduced flux quantum, and M is the mutual inductance. Other parameters are $E_C = e^2/(2C)$ and $E_L = \Phi_0^2/L$. Here, Q and Φ satisfy the commutation relations $[\Phi, Q] = i$. When $\Phi_e/\Phi_0 = \pi$ and $E_L < E_J$, the anharmonicity of the Hamiltonian H_0 is positive and can be adjusted to a large value [104,107].

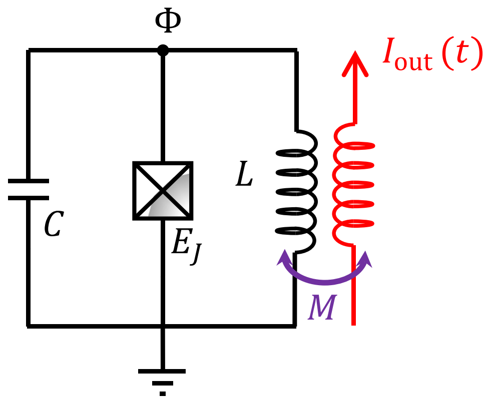

FIG. 8. Circuit of a fluxonium qubit, which is formed by a capacitor C, an inductor L, and a Josephson junction with Josephson energy E_J. The qubit is controlled by an external current $I_{\rm out}(t)$, which couples to the dimensionless flux variable Φ through a mutual inductance M.

According to the experiment in Ref. [104], we can choose $E_J/(2\pi) = 5$ GHz, $E_C/(2\pi) = 0.8$ GHz, and $E_L/(2\pi) = 1.1$ GHz, resulting in $\omega_{01}/(2\pi) = 0.3$ GHz and $\omega_{12}/(2\pi) = 3.5$ GHz, where ω_{01} (ω_{12}) is the level transition frequency of the first (second) and second (third) eigenstates of H_0. The spontaneous emission and dephasing rates are $\gamma = 2\pi \times 0.6$ kHz and $\gamma_\phi = 2\pi \times 1.1$ kHz [104], respectively. Then, by accordingly choosing the parameters for the driving Hamiltonian $H_D(t)$, we can obtain the total Hamiltonian in Eq. (1), and thus, to realize our protocol.

IX. CONCLUSIONS AND OUTLOOK

We show that employing CR effects (using the CHRW and the RWA-BS protocols) can effectively improve the speed and fidelity of geometric quantum computation. When CR effects are considered in implementing single- and two-qubit gates, it is allowed to apply strong driving fields with amplitudes, which are comparable to the atomic transition frequencies. This significantly improves the gate speed, and, thus, reducing the influence of decoherence. Moreover, because the CR effects (e.g., the BS shift) are not neglected, we can avoid the additional dynamical noise induced by such an effect and further improve the gate fidelity. No specific design for the driving fields is required in the proposed protocol, and, thus, the protocol is compatible with most optimal control experimental methods used in previous works. The proposed protocol also can be generalized to multiqubit systems using strong couplings. Another application of the proposed protocol can be to multilevel (qudit) systems, such as a Λ-type system [33,48,64,65], which are compatible with other control methods to improve the speed and fidelity of quantum computation. All these advantages make our protocol possible to accelerate the previous RWA-based geometric and holonomic quantum computation, so as to improve the fidelity of the computation.

ACKNOWLEDGMENTS

We acknowledge helpful discussions with Yi-Hao Kang and Jiang Zhang. Y.-H.C. is supported by the Japan Society for the Promotion of Science (JSPS) KAKENHI Grant No. JP19F19028. A.M. is supported by the Polish National Science Centre (NCN) under the Maestro Grant No. DEC-2019/34/A/ST2/00081. X.C. is supported by EU FET Open Grant EPIQUS (899368), QUANTEK Project (KK-2021/00070), the Basque Government through Grant No. IT1470-22, the Project Grant PID2021-126273NB-I00 funded by MCIN/AEI/10.13039/501100011033 and by “ERDF A way of making Europe” and “ERDF Invest in your Future” and the Ramón y Cajal program (RYC-2017-22482). Y.X. is supported by the National Natural Science Foundation of China under Grant No. 11575045, the Natural Science Funds for Distinguished Young Scholar of Fujian Province under Grant No. 2020J06011 and Project from Fuzhou University under Grant No. JG202001-2. F.N. is supported in part by Nippon Telegraph and Telephone Corporation (NTT) Research, the Japan Science and Technology Agency (JST) [via the Quantum Leap Flagship Program (Q-LEAP), and the Moonshot R&D Grant No. JPMJMS2061], the Japan Society for the Promotion of Science (JSPS) [via the Grants-in-Aid for Scientific Research (KAKENHI) Grant No. JP20H00134], the Army Research Office (ARO) (Grant No. W911NF-18-1-0358), the Asian Office of Aerospace Research and Development (AOARD) (via Grant No. FA2386-20-1-4069), and the Foundational Questions Institute Fund (FQXi) via Grant No. FQXi-IAF19-06.

APPENDIX A: INVARIANT-BASED ENGINEERING

For an arbitrary Hamiltonian $H(t)$, we can find a dynamical invariant $I(t)$ satisfying

$$i\frac{\partial I(t)}{\partial t} - [H(t), I(t)] = 0, \tag{A1}$$

so that the expectation values of $I(t)$ remain constant. According to the Lewis-Risenfeld theory [72], the solution of the Schrödinger equation

$$i\frac{\partial}{\partial t}|\psi(t)\rangle = H(t)|\psi(t)\rangle, \tag{A2}$$

can be expressed as a superposition of the eigenstates of the invariant $I(t)$ as

$$|\psi(t)\rangle = \sum_n c_n \exp\left[i\mathcal{R}_n(t)\right]|\mathcal{I}_n(t)\rangle, \tag{A3}$$

where c_n are time-independent amplitudes, $|\mathcal{I}_n\rangle$ are the eigenstates of $I(t)$, and $\mathcal{R}_n(t)$ are the Lewis-Risenfeld phases:

$$\mathcal{R}_n(t) = \int_0^t \left\langle \mathcal{I}_n(t') \left| \frac{\partial}{\partial t'} - H(t') \right| \mathcal{I}_n(t') \right\rangle dt'. \tag{A4}$$

For the effective two-level Hamiltonians in Eqs. (3) and (23), the invariant $I(t)$ is found to be

$$I(t) = \Xi_0 \begin{bmatrix} -\cos\beta & i\sin\beta\exp(-i\alpha) \\ -i\sin\beta\exp(i\alpha) & \cos\beta \end{bmatrix}, \tag{A5}$$

where Ξ_0 is a constant to keep $I(t)$ with dimensions of frequency. The eigenstates of $I(t)$ are

$$|\mathcal{I}_+(t)\rangle = \begin{bmatrix} i\sin\left(\frac{\beta}{2}\right)\exp(-i\alpha) \\ \cos\left(\frac{\beta}{2}\right) \end{bmatrix}, \quad |\mathcal{I}_-(t)\rangle = \begin{bmatrix} \cos\left(\frac{\beta}{2}\right) \\ i\sin\left(\frac{\beta}{2}\right)\exp(i\alpha) \end{bmatrix}. \tag{A6}$$

Thus, we obtain the evolution paths in Eqs. (17) and (18), which are

$$|\phi_\pm(t)\rangle = \exp[i\mathcal{R}_\pm(t)]|\mathcal{I}_\pm(t)\rangle. \tag{A7}$$

The relationships of the parameters can be obtained by substituting Eqs. (3), (23), and (A5) into Eq. (A1). Thus, we obtain Eqs. (17)–(19).

[1] S. Aaronson and A. Arkhipov, in *Proceedings of the 43rd annual ACM symposium on Theory of computing* (ACM Press, New York, 2011), p. 333.

[2] E. Farhi, J. Goldstone, S. Gutmann, and L. Zhou, The quantum approximate optimization algorithm and the Sherrington-Kirkpatrick model at infinite size, Quantum **6**, 759 (2022).

[3] J. D. Hidary, *Quantum Computing: An Applied Approach* (Springer, Berlin, 2019).

[4] A. F. Kockum and F. Nori, in *Fundamentals and Frontiers of the Josephson Effect*, edited by F. Tafuri (Springer, Berlin, 2019), Chap. 17, Vol. 286, p. 703.

[5] M. Kjaergaard, M. E. Schwartz, J. Braumüller, P. Krantz, J. I.-J. Wang, S. Gustavsson, and W. D. Oliver, Superconducting qubits: Current state of play, Ann. Rev. Cond. Matt. Phys. **11**, 369 (2020).

[6] H.-S. Zhong *et al.*, Quantum computational advantage using photons, Science **370**, 1460 (2020).

[7] R. J. Lipton and K. W. Regan, *Introduction to Quantum Algorithms via Linear Algebra* (The MIT Press, Cambridge, 2021).

[8] Y. Nakamura, Y. A. Pashkin, and J. S. Tsai, Coherent control of macroscopic quantum states in a single-Cooper-pair box, Nature (London) **398**, 786 (1999).

[9] Y. Nakamura, Y. A. Pashkin, and J. S. Tsai, Rabi Oscillations in a Josephson-Junction Charge Two-Level System, Phys. Rev. Lett. **87**, 246601 (2001).

[10] Y. Makhlin, G. Schön, and A. Shnirman, Quantum-state engineering with Josephson-junction devices, Rev. Mod. Phys. **73**, 357 (2001).

[11] J. Q. You, J. S. Tsai, and F. Nori, Scalable Quantum Computing with Josephson Charge Qubits, Phys. Rev. Lett. **89**, 197902 (2002).

[12] J. Q. You, J. S. Tsai, and F. Nori, Controllable manipulation and entanglement of macroscopic quantum states in coupled charge qubits, Phys. Rev. B **68**, 024510 (2003).

[13] L. F. Wei, Y.-x. Liu, and F. Nori, Quantum computation with Josephson qubits using a current-biased information bus, Phys. Rev. B **71**, 134506 (2005).

[14] I. Buluta, S. Ashhab, and F. Nori, Natural and artificial atoms for quantum computation, Rep. Prog. Phys. **74**, 104401 (2011).

[15] X. Gu *et al.*, Microwave photonics with superconducting quantum circuits, Phys. Rep. **718-719**, 1 (2017).

[16] C. D. Bruzewicz, J. Chiaverini, R. McConnell, and J. M. Sage, Trapped-ion quantum computing: Progress and challenges, Appl. Phys. Rev. **6**, 021314 (2019).

[17] H.-L. Huang, D. Wu, D. Fan, and X. Zhu, Superconducting quantum computing: A review, Sci. China Inf. Sci. **63**, 180501 (2020).

[18] W. Cai, Y. Ma, W. Wang, C.-L. Zou, and L. Sun, Bosonic quantum error correction codes in superconducting quantum circuits, Fund. Res. **1**, 50 (2021).

[19] P. Zanardi and M. Rasetti, Holonomic quantum computation, Phys. Lett. A **264**, 94 (1999).

[20] A. Ekert, M. Ericsson, P. Hayden, H. Inamori, J. A. Jones, D. K. L. Oi, and V. Vedral, Geometric quantum computation, J. Mod. Opt. **47**, 2501 (2000).

[21] J. A. Jones, V. Vedral, A. Ekert, and G. Castagnoli, Geometric quantum computation using nuclear magnetic resonance, Nature **403**, 869 (2000).

[22] X.-B. Wang and K. Matsumoto, Nonadiabatic Conditional Geometric Phase Shift with NMR, Phys. Rev. Lett. **87**, 097901 (2001).

[23] S.-L. Zhu and Z. D. Wang, Unconventional Geometric Quantum Computation, Phys. Rev. Lett. **91**, 187902 (2003).

[24] S.-L. Zhu and P. Zanardi, Geometric quantum gates that are robust against stochastic control errors, Phys. Rev. A **72**, 020301(R) (2005).

[25] S. Filipp, J. Klepp, Y. Hasegawa, C. Plonka-Spehr, U. Schmidt, P. Geltenbort, and H. Rauch, Experimental Demonstration of the Stability of Berry's Phase for a Spin-1/2 Particle, Phys. Rev. Lett. **102**, 030404 (2009).

[26] E. Sjöqvist, D. M. Tong, L. M. Andersson, B. Hessmo, M. Johansson, and K. Singh, Non-adiabatic holonomic quantum computation, New J. Phys. **14**, 103035 (2012).

[27] S. Berger, M. Pechal, A. A. Abdumalikov, C. Eichler, L. Steffen, A. Fedorov, A. Wallraff, and S. Filipp, Exploring the effect of noise on the Berry phase, Phys. Rev. A **87**, 060303(R) (2013).

[28] G. F. Xu, J. Zhang, D. M. Tong, E. Sjöqvist, and L. C. Kwek, Nonadiabatic holonomic quantum computation in decoherence-free subspaces, Phys. Rev. Lett. **109**, 170501 (2012).

[29] E. Sjöqvist, Geometric phases in quantum information, Int. J. Quantum Chem. **115**, 1311 (2015).

[30] S.-B. Zheng, C.-P. Yang, and F. Nori, Comparison of the sensitivity to systematic errors between nonadiabatic non-Abelian geometric gates and their dynamical counterparts, Phys. Rev. A **93**, 032313 (2016).

[31] P. Z. Zhao, X.-D. Cui, G. F. Xu, E. Sjöqvist, and D. M. Tong, Rydberg-atom-based scheme of nonadiabatic geometric quantum computation, Phys. Rev. A **96**, 052316 (2017).

[32] Y. Xu, W. Cai, Y. Ma, X. Mu, L. Hu, T. Chen, H. Wang, Y. P. Song, Z.-Y. Xue, Z.-q. Yin, and L. Sun, Single-Loop Realization of Arbitrary Nonadiabatic Holonomic Single-Qubit Quantum Gates in a Superconducting Circuit, Phys. Rev. Lett. **121**, 110501 (2018).

[33] B.-J. Liu, X.-K. Song, Z.-Y. Xue, X. Wang, and M.-H. Yung, Plug-and-Play Approach to Nonadiabatic Geometric Quantum Gates, Phys. Rev. Lett. **123**, 100501 (2019).

[34] J. Zeng, C. H. Yang, A. S. Dzurak, and E. Barnes, Geometric formalism for constructing arbitrary single-qubit dynamically corrected gates, Phys. Rev. A **99**, 052321 (2019).

[35] Y. Xu, Z. Hua, T. Chen, X. Pan, X. Li, J. Han, W. Cai, Y. Ma, H. Wang, Y. P. Song, Z.-Y. Xue, and L. Sun, Experimental Implementation of Universal Nonadiabatic Geometric Quantum Gates in a Superconducting Circuit, Phys. Rev. Lett. **124**, 230503 (2020).

[36] B.-J. Liu, S.-L. Su, and M.-H. Yung, Nonadiabatic noncyclic geometric quantum computation in Rydberg atoms, Phys. Rev. Res. **2**, 043130 (2020).

[37] W. Dong, F. Zhuang, S. E. Economou, and E. Barnes, Doubly Geometric Quantum Control, PRX Quantum **2**, 030333 (2021).

[38] B.-J. Liu, Y.-S. Wang, and M.-H. Yung, Super-robust nonadiabatic geometric quantum control, Phys. Rev. Res. **3**, L032066 (2021).

[39] J. Zhang, T. H. Kyaw, S. Filipp, L.-C. Kwek, E. Sjöqvist, and D. M. Tong, Geometric and holonomic quantum computation, arXiv:2110.03602.

[40] M. V. Berry, Quantal phase factors accompanying adiabatic changes, Proc. Roy. Soc. Lond. A **392**, 45 (1984).

[41] Y. Aharonov and J. Anandan, Phase Change During a Cyclic Quantum Evolution, Phys. Rev. Lett. **58**, 1593 (1987).

[42] J. Anandan, Non-adiabatic non-Abelian geometric phase, Phys. Lett. A **133**, 171 (1988).

[43] G. De Chiara and G. M. Palma, Berry Phase for a Spin 1/2 Particle in a Classical Fluctuating Field, Phys. Rev. Lett. **91**, 090404 (2003).

[44] X.-K. Song, H. Zhang, Q. Ai, J. Qiu, and F.-G. Deng, Shortcuts to adiabatic holonomic quantum computation in decoherence-free subspace with transitionless quantum driving algorithm, New J. Phys. **18**, 023001 (2016).

[45] Y. Du, Z. Liang, H. Yan, and S.-L. Zhu, Geometric quantum computation with shortcuts to adiabaticity, Adv. Quantum Tech. **2**, 1900013 (2019).

[46] S. Li, P. Shen, T. Chen, and Z.-Y. Xue, Noncyclic nonadiabatic holonomic quantum gates via shortcuts to adiabaticity, Front. Phys. **16**, 51502 (2021).

[47] Y.-H. Chen, W. Qin, R. Stassi, X. Wang, and F. Nori, Fast binomial-code holonomic quantum computation with ultrastrong light-matter coupling, Phys. Rev. Res. **3**, 033275 (2021).

[48] F. Setiawan, P. Groszkowski, H. Ribeiro, and A. A. Clerk, Analytic Design of Accelerated Adiabatic Gates in Realistic Qubits: General Theory and Applications to Superconducting Circuits, PRX Quantum **2**, 030306 (2021).

[49] P. Shen, T. Chen, and Z.-Y. Xue, Ultrafast Holonomic Quantum Gates, Phys. Rev. Appl. **16**, 044004 (2021).

[50] Y. Wang, J. Zhang, C. Wu, J. Q. You, and G. Romero, Holonomic quantum computation in the ultrastrong-coupling regime of circuit QED, Phys. Rev. A **94**, 012328 (2016).

[51] Y. Wang, C. Guo, G.-Q. Zhang, G. Wang, and C. Wu, Ultrafast quantum computation in ultrastrongly coupled circuit QED systems, Sci. Rep. **7**, 44251 (2017).

[52] Y. Wang, Y. Su, X. Chen, and C. Wu, Dephasing-Protected Scalable Holonomic Quantum Computation on a Rabi Lattice, Phys. Rev. Appl. **14**, 044043 (2020).

[53] F. Casas, J. A. Oteo, and J. Ros, Floquet theory: exponential perturbative treatment, J. Phys. A **34**, 3379 (2001).

[54] S. Ashhab *et al.*, Two-level systems driven by large-amplitude fields, Phys. Rev. A **75**, 063414 (2007).

[55] Zhiguo Lü and Hang Zheng, Effects of counter-rotating interaction on driven tunneling dynamics: Coherent destruction of tunneling and Bloch-Siegert shift, Phys. Rev. A **86**, 023831 (2012).

[56] N. Goldman and J. Dalibard, Periodically Driven Quantum Systems: Effective Hamiltonians and Engineered Gauge Fields, Phys. Rev. X **4**, 031027 (2014).

[57] Y. Yan, Z. Lü, and H. Zheng, Bloch-Siegert shift of the Rabi model, Phys. Rev. A **91**, 053834 (2015).

[58] C. Deng, F. Shen, S. Ashhab, and A. Lupascu, Dynamics of a two-level system under strong driving: Quantum-gate optimization based on Floquet theory, Phys. Rev. A **94**, 032323 (2016).

[59] Y. Han, X.-Q. Luo, T.-F. Li, and W. Zhang, Analytical double-unitary-transformation approach for strongly and periodically driven three-level systems, Phys. Rev. A **101**, 022108 (2020).

[60] J. H. Shirley, Solution of the Schrödinger equation with a Hamiltonian periodic in time, Phys. Rev. **138**, B979 (1965).

[61] J. Tuorila, M. Silveri, M. Sillanpää, E. Thuneberg, Y. Makhlin, and P. Hakonen, Stark Effect and Generalized Bloch-Siegert Shift in a Strongly Driven Two-Level System, Phys. Rev. Lett. **105**, 257003 (2010).

[62] B. T. Torosov, S. Guérin, and N. V. Vitanov, High-Fidelity Adiabatic Passage by Composite Sequences of Chirped Pulses, Phys. Rev. Lett. **106**, 233001 (2011).

[63] E. Herterich and E. Sjöqvist, Single-loop multiple-pulse nonadiabatic holonomic quantum gates, Phys. Rev. A **94**, 052310 (2016).

[64] P. Z. Zhao, G. F. Xu, Q. M. Ding, E. Sjöqvist, and D. M. Tong, Single-shot realization of nonadiabatic holonomic

quantum gates in decoherence-free subspaces, Phys. Rev. A **95**, 062310 (2017).
[65] F. Zhang, J. Zhang, P. Gao, and G. Long, Searching nonadiabatic holonomic quantum gates via an optimization algorithm, Phys. Rev. A **100**, 012329 (2019).
[66] G. Dridi, K. Liu, and S. Guérin, Optimal Robust Quantum Control by Inverse Geometric Optimization, Phys. Rev. Lett. **125**, 250403 (2020).
[67] V. A. Mousolou, C. M. Canali, and E. Sjöqvist, Universal non-adiabatic holonomic gates in quantum dots and single-molecule magnets, New J. Phys. **16**, 013029 (2014).
[68] V. A. Mousolou, Electric nonadiabatic geometric entangling gates on spin qubits, Phys. Rev. A **96**, 012307 (2017).
[69] J. J. W. H. Sørensen, M. Dalgaard, A. H. Kiilerich, K. Mølmer, and J. F. Sherson, Quantum control with measurements and quantum zeno dynamics, Phys. Rev. A **98**, 062317 (2018).
[70] P. Zanardi and D. A. Lidar, Purity and state fidelity of quantum channels, Phys. Rev. A **70**, 012315 (2004).
[71] L. H. Pedersen, N. M. Møller, and K. Mølmer, Fidelity of quantum operations, Phys. Lett. A **367**, 47 (2007).
[72] H. R. Lewis and W. B. Riesenfeld, An exact quantum theory of the time-dependent harmonic oscillator and of a charged particle in a time-dependent electromagnetic field, J. Math. Phys. **10**, 1458 (1969).
[73] X. Chen, E. Torrontegui, and J. G. Muga, Lewis-Riesenfeld invariants and transitionless quantum driving, Phys. Rev. A **83**, 062116 (2011).
[74] X. Chen, I. Lizuain, A. Ruschhaupt, D. Guéry-Odelin, and J. G. Muga, Shortcut to Adiabatic Passage in Two- and Three-Level Atoms, Phys. Rev. Lett. **105**, 123003 (2010).
[75] S. Ibáñez, X. Chen, E. Torrontegui, J. G. Muga, and A. Ruschhaupt, Multiple Schrödinger Pictures and Dynamics in Shortcuts to Adiabaticity, Phys. Rev. Lett. **109**, 100403 (2012).
[76] E. Torrontegui, S. Ibáñez, S. Martínez-Garaot, M. Modugno, A. del Campo, D. Guéry-Odelin, A. Ruschhaupt, X. Chen, and J. G. Muga, in *Adv. At. Mol. Opt. Phys.* (Elsevier, 2013), p. 117.
[77] D. Guéry-Odelin, A. Ruschhaupt, A. Kiely, E. Torrontegui, S. Martínez-Garaot, and J. G. Muga, Shortcuts to adiabaticity: Concepts, methods, and applications, Rev. Mod. Phys. **91**, 045001 (2019).
[78] A. Steane, Multiple-particle interference and quantum error correction, Proc. Roy. Soc. Lond. A **452**, 2551 (1996).
[79] H. P. Breuer and F. Petruccione, *The Theory of Open Quantum Systems* (Oxford University Press, Oxford, 2007).
[80] D. A. Lidar, Lecture notes on the theory of open quantum systems, arXiv:1902.00967.
[81] Z.-L. Xiang *et al.*, Hybrid quantum circuits: Superconducting circuits interacting with other quantum systems, Rev. Mod. Phys. **85**, 623 (2013).
[82] Q.-C. Wu, Y.-H. Zhou, B.-L. Ye, T. Liu, and C.-P. Yang, Nonadiabatic quantum state engineering by time-dependent decoherence-free subspaces in open quantum systems, New J. Phys. **23**, 113005 (2021).
[83] P. W. Shor, Scheme for reducing decoherence in quantum computer memory, Phys. Rev. A **52**, R2493 (1995).
[84] D. Gottesman, in *Quantum information science and its contributions to mathematics, Proc. Sym. Appl. Math.* (2010), Vol. 68 , p. 13.
[85] L. Qiu, H. Li, Z. Han, W. Zheng, X. Yang, Y. Dong, S. Song, D. Lan, X. Tan, and Y. Yu, Experimental realization of noncyclic geometric gates with shortcut to adiabaticity in a superconducting circuit, Appl. Phys. Lett. **118**, 254002 (2021).
[86] K. Xu, W. Ning, X.-J. Huang, P.-R. Han, H. Li, Z.-B. Yang, D. Zheng, H. Fan, and S.-B. Zheng, Demonstration of a non-Abelian geometric controlled-NOT gate in a superconducting circuit, Optica **8**, 972 (2021).
[87] M. Grajcar *et al.*, Four-qubit device with mixed couplings, Phys. Rev. Lett. **96**, 047006 (2006).
[88] A. O. Niskanen, K. Harrabi, F. Yoshihara, Y. Nakamura, and J. S. Tsai, Spectroscopy of three strongly coupled flux qubits, Phys. Rev. B **74**, 220503(R) (2006).
[89] R. Harris, T. Lanting, A. J. Berkley, J. Johansson, M. W. Johnson, P. Bunyk, E. Ladizinsky, N. Ladizinsky, T. Oh, and S. Han, Compound Josephson-junction coupler for flux qubits with minimal crosstalk, Phys. Rev. B **80**, 052506 (2009).
[90] S. Richer and D. DiVincenzo, Circuit design implementing longitudinal coupling: A scalable scheme for superconducting qubits, Phys. Rev. B **93**, 134501 (2016).
[91] S. Richer, N. Maleeva, S. T. Skacel, I. M. Pop, and D. DiVincenzo, Inductively shunted transmon qubit with tunable transverse and longitudinal coupling, Phys. Rev. B **96**, 174520 (2017).
[92] L. Garziano *et al.*, One Photon Can Simultaneously Excite Two or More Atoms, Phys. Rev. Lett. **117**, 043601 (2016).
[93] X. Wang *et al.*, Observing pure effects of counter-rotating terms without ultrastrong coupling: A single photon can simultaneously excite two qubits, Phys. Rev. A **96**, 063820 (2017).
[94] X. Wang *et al.*, Two-color electromagnetically induced transparency via modulated coupling between a mechanical resonator and a qubit, Phys. Rev. A **98**, 023821 (2018).
[95] R. Stassi and F. Nori, Long-lasting quantum memories: Extending the coherence time of superconducting artificial atoms in the ultrastrong-coupling regime, Phys. Rev. A **97**, 033823 (2018).
[96] J. Clarke and F. K. Wilhelm, Superconducting quantum bits, Nature (London) **453**, 1031 (2008).
[97] J. Q. You and F. Nori, Atomic physics and quantum optics using superconducting circuits, Nature **474**, 589 (2011).
[98] P. D. Nation, J. R. Johansson, M. P. Blencowe, and F. Nori, Colloquium: Stimulating uncertainty: Amplifying the quantum vacuum with superconducting circuits, Rev. Mod. Phys. **84**, 1 (2012).
[99] G. Wendin, Quantum information processing with superconducting circuits: A review, Rep. Prog. Phys. **80**, 106001 (2017).

[100] A. F. Kockum, A. Miranowicz, S. De Liberato, S. Savasta, and F. Nori, Ultrastrong coupling between light and matter, Nat. Rev. Phys. **1**, 19 (2019).

[101] P. Forn-Díaz, L. Lamata, E. Rico, J. Kono, and E. Solano, Ultrastrong coupling regimes of light-matter interaction, Rev. Mod. Phys. **91**, 025005 (2019).

[102] C. Deng, J.-L. Orgiazzi, F. Shen, S. Ashhab, and A. Lupascu, Observation of Floquet States in a Strongly Driven Artificial Atom, Phys. Rev. Lett. **115**, 133601 (2015).

[103] J. E. Mooij, T. P. Orlando, L. Levitov, L. Tian, C. H. van der Wal, and S. Lloyd, Josephson persistent-current qubit, Science **285**, 1036 (1999).

[104] L. B. Nguyen, Y.-H. Lin, A. Somoroff, R. Mencia, N. Grabon, and V. E. Manucharyan, High-Coherence Fluxonium Qubit, Phys. Rev. X **9**, 041041 (2019).

[105] T. Niemczyk *et al.*, Circuit quantum electrodynamics in the ultrastrong-coupling regime, Nat. Phys. **6**, 772 (2010).

[106] P. Forn-Díaz, J. Lisenfeld, D. Marcos, J. J. García-Ripoll, E. Solano, C. J. P. M. Harmans, and J. E. Mooij, Observation of the Bloch-Siegert Shift in a Qubit-Oscillator System in the Ultrastrong Coupling Regime, Phys. Rev. Lett. **105**, 237001 (2010).

[107] D. Zhu, T. Jaako, Q. He, and P. Rabl, Quantum Computing with Superconducting Circuits in the Picosecond Regime, Phys. Rev. Appl. **16**, 014024 (2021).